INSTITUTE OF PHYSICS PUBLISHING JOURNAL OF PHYSICS: CONDENSED MATTER

J. Phys.: Condens. Matter **18** (2006) 9549–9560 doi:10.1088/0953-8984/18/42/002

Luminescence of Ce^{3+} activated fluoro-apatites $M_5(PO_4)_3F$ (M = Ca, Sr, Ba) under VUV–UV and x-ray excitation

Qu Zeng[1], Hongbin Liang[1,4], Guobin Zhang[2], M Danang Birowosuto[3], Zifeng Tian[1], Huihong Lin[1], Yibing Fu[2], Pieter Dorenbos[3] and Qiang Su[1]

[1] MOE Laboratory of Bioinorganic and Synthetic Chemistry, State Key Laboratory of Optoelectronic Materials and Technologies, School of Chemistry and Chemical Engineering, Sun Yat-sen University, Guangzhou 510275, People's Republic of China
[2] National Synchrotron Radiation Laboratory, University of Science and Technology of China, Hefei 230026, People's Republic of China
[3] Faculty of Applied Sciences, Delft University of Technology, Mekelweg 15, 2629 JB Delft, The Netherlands

E-mail: cesbin@mail.sysu.edu.cn

Received 6 July 2006, in final form 14 September 2006
Published 5 October 2006
Online at stacks.iop.org/JPhysCM/18/9549

Abstract

Fluoro-apatite $M_5(PO_4)_3F$ (M = Ca, Sr, Ba) phosphors activated with Ce^{3+} ions were prepared by a solid state reaction technique at high temperature. The excitation spectra in the VUV (vacuum ultraviolet)–UV range and the emission spectra in the UV–vis range together with decay time spectra are investigated and discussed. X-ray excited emission spectra were measured and light yields are calculated. The results revealed that Ca(II) sites are preferentially occupied at low doping concentration, and then Ca(I) sites are dominant with the increasing of concentration for Ce^{3+} in $Ca_5(PO_4)_3F$. In contrast, Ce^{3+} ions mainly occupied the Sr(II)/Ba(II) sites in $Sr_5(PO_4)_3F$ and $Ba_5(PO_4)_3F$ even at higher doping concentration. The low light output seems to suggest that the materials are not suitable x-ray or gamma-ray phosphors.

(Some figures in this article are in colour only in the electronic version)

1. Introduction

The halo-apatites are effective host lattices for luminescence and laser materials. The optical properties of these classes of compounds have been the subject of numerous investigations. Outstanding examples are the Sb^{3+} and Mn^{2+} co-doped calcium halo-apatites $Ca_5(PO_4)_3X:Sb^{3+}$, Mn^{2+} (X = F, Cl) which are well-known phosphors in fluorescent

[4] Author to whom any correspondence should be addressed.

lamps. In the last decades, most efforts were devoted to the investigation of the luminescent properties of halo-apatites doped with rare earth ions, and many halo-apatites with interesting spectroscopic properties were found [1–6]. However, the luminescent properties of Ce^{3+} activated fluoro-apatites $M_5(PO_4)_3F{:}Ce^{3+}$ (M = Ca, Sr, Ba) upon VUV (vacuum ultraviolet, $E > 50\,000\ cm^{-1}$, $\lambda < 200$ nm) and x-ray excitation have not received attention to the best of our knowledge, though those upon UV excitation have been studied [2, 4, 5].

For rare earth activated phosphors, four types of electronic transition may occur in the VUV range, i.e. (1) intra-configurational 4f–4f transitions, (2) inter-configurational 4f–5d transitions, (3) charge transfer transitions from the ligand anions to the rare earth ions, and (4) electronic excitation of host anions (host-related transitions) [7]. The 5d states of rare earth ions are outer orbital, and the coordination around the lanthanide ion has profound influence on their energies. As a result the 4f–5d transitions appear in a wavelength range that depends strongly on both the type of rare earth ion and the type of host lattice. The 4f–5d transitions are parity allowed and together with a strong 5d-electron–lattice coupling it leads to broad absorption bands with large optical absorption cross-section. Clearly, the 4f–5d transitions absorb excitation energy more efficiently than the parity-forbidden sharp line-like 4f–4f transitions. Hence the experimental investigation on the 4f–5d transitions of rare earth ions in the VUV range is important in the search for novel efficient phosphors.

In the present paper, the luminescence properties of the Ce^{3+} doped fluoro-apatites $M_5(PO_4)_3F$ (M = Ca, Sr, Ba) under VUV–UV and x-ray excitation are reported.

2. Experimental details

A series of powder samples of $M_{5-2x}Ce_xNa_x(PO_4)_3F$ (for M = Ca, Sr, Ba; $x = 0$, 0.005, 0.01, 0.015, 0.02, 0.025, 0.035, 0.05, 0.15, 0.20, 0.25, 0.30, 0.35, 0.40) were prepared by a high-temperature solid-state reaction technique using the following reactions.

$$4(1-x)MCO_3 + 6MHPO_4{\cdot}2H_2O + 2NH_4F + 2xCeO_2 + xNa_2CO_3 + xCO \xrightarrow{1373\ K/2\ h} 2M_{5-2x}Ce_xNa_x(PO_4)_3F + 2NH_3 + 16H_2O + 2(2-x)CO_2,$$

for M = Ca, Sr

$$2(5-2x)Ba(NO_3)_2 + 6(NH_4)_2HPO_4 + 2NH_4F + 2xCeO_2 + xNa_2CO_3 + (10-3x)CO \xrightarrow{1373\ K/2\ h} 2Ba_{5-2x}Ce_xNa_x(PO_4)_3F + 14NH_3 + 10H_2O + 2(5-x)CO_2 + 2(5-2x)NO_2.$$

Stoichiometric mixtures of analytical-grade purity MCO_3 and $MHPO_4{\cdot}2H_2O$ (for M = Ca, Sr) (or $Ba(NO_3)_2$ and $(NH_4)_2HPO_4$), Na_2CO_3, NH_4F (excess 10 mol%) and 99.9% purity CeO_2 were heated at 1100 °C for 2 h under CO reducing atmosphere. The final products were obtained by washing the samples with distilled water and then drying. Because trivalent Ce^{3+} ions are located on the lattice sites of divalent M^{2+} ions, Na^+ ions were added as a charge-compensating defect. Different types of reactant (carbonates $CaCO_3/SrCO_3$, and nitrate $Ba(NO_3)_2$) were used when we prepared $M_{5-2x}Ce_xNa_x(PO_4)_3F$, because we cannot obtain a final product with pure single phase for M = Ba using $BaCO_3$.

The structure of the final products was examined by x-ray powder diffraction using Cu Kα radiation on a Rigaku D/max 2200 vpc x-ray diffractometer. For the measurements on the spectroscopic properties, the spectra in the UV–vis range for all samples were first recorded on a Jobin Yvon FL3-21 spectrofluorometer at room temperature, and then the samples with strong luminescence were chosen to examine the VUV spectra, the decay time and the x-ray excited luminescent properties. The VUV–UV excitation spectra and the luminescent spectra under

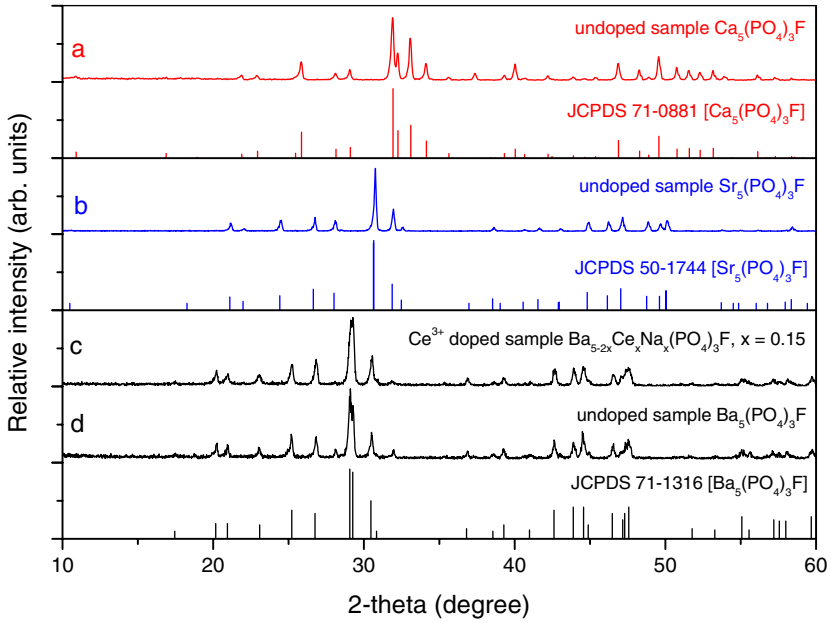

Figure 1. The XRD patterns of samples $M_5(PO_4)_3F$ for M = Ca, Sr, Ba.

VUV–UV excitation were measured at the time-resolved spectroscopy experimental station on beam line U24 of the National Synchrotron Radiation Laboratory (NSRL). The luminescence decay curves were recorded on an Edinburgh FLS 920 spectrofluorometer. The details of these measurements were described in our previous work [8, 9].

X-ray excited emission spectra were recorded using an x-ray tube with Cu anode operating at 35 kV and 25 mA. The emission of the sample was dispersed by means of an Acton Research Company (ARC) VM-504 monochromator (blazed at 300 nm, 1200 groves mm^{-1}) and detected by a Hamamatsu R934-04 PMT (Photo-multiplier Tube). The slit width was 1 mm. The spectra were corrected for the wavelength dependence of the photomultiplier quantum efficiency as well as for the monochromator transmission. To determine the absolute photon output of the material we compared the emission with that of a BaF_2 reference crystal measured under identical conditions. The light yield of BaF_2 was determined independently by means of gamma-ray excitation using standard scintillation detection techniques.

3. Results and discussion

3.1. The x-ray diffraction patterns

X-ray diffraction (XRD) patterns of the series of phosphors $M_{5-2x}Ce_xNa_x(PO_4)_3F$ (for M = Ca, Sr, Ba; $x = 0$, 0.025, 0.05, 0.10, 0.15, 0.20, 0.25, 0.30, 0.35, 0.40) were obtained. As examples, the XRD patterns of undoped samples $M_5(PO_4)_3F$ (M = Ca, Sr, Ba) and a Ce^{3+} doped sample $Ba_{5-2x}Ce_xNa_x(PO_4)_3F$ for $x = 0.15$ are shown in figure 1 and compared with that of JCPDS standard cards, respectively. Among divalent alkaline earth M^{2+} (M = Ca, Sr, Ba), Ba^{2+} ions have the largest ionic size; the ionic radius difference between M^{2+} and Ce^{3+} is also the biggest for M = Ba. So the XRD patterns of a Ce^{3+} doped Ba-containing sample are also shown in figure 1. Diffractograms a, b and c, d are consistent with JCPDS standard

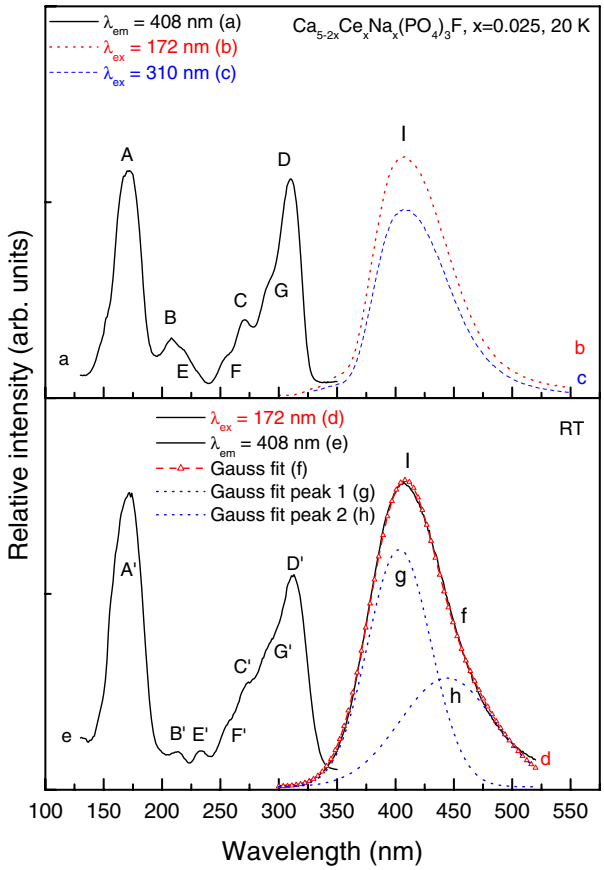

Figure 2. The VUV excitation and emission spectra for samples $Ca_{5-2x}Ce_xNa_x(PO_4)_3F$ ($x = 0.025$) at 20 K and room temperature (RT).

cards numbered 71-0881 [$Ca_5(PO_4)_3F$], 50-1744 [$Sr_5(PO_4)_3F$], and 71-1316 [$Ba_5(PO_4)_3F$], respectively. The XRD patterns of other Ce^{3+} doped samples $M_{5-2x}Ce_xNa_x(PO_4)_3F$ are not displayed in the figure, but we found that those patterns are in line with those of undoped samples $M_5(PO_4)_3F$, suggesting that the dopant Ce^{3+} and Na^+ do not significantly influence the XRD patterns. In comparison diffractograms a, b with c, d, it seems that the Ba-samples are with lower crystallinity than Ca- and Sr-samples. This may be due to (1) the different raw materials being used for preparation of Ba-samples and Ca-/Sr-samples, (2) the largest ionic size of Ba^{2+} and (3) the largest ionic radius difference between Ba^{2+} and Ce^{3+} as we mentioned in the experimental section. However, from figure 1 we can conclude that all samples $M_{5-2x}Ce_xNa_x(PO_4)_3F$ are of single $M_5(PO_4)_3F$ (M = Ca, Sr, Ba) phase.

3.2. VUV–vis luminescence of $Ca_5(PO_4)_3F$:Ce

Figure 2 shows the excitation spectra in the 130–350 nm range and the emission spectra in the 300–550 nm range for samples $Ca_{5-2x}Ce_xNa_x(PO_4)_3F$ ($x = 0.025$) at 20 K and at room temperature (RT). Curve (a) is the excitation spectrum in the range from 130 to 350 nm at 20 K obtained by monitoring the emission at 408 nm. Four broad bands, which are marked as A (172 nm), B (209 nm), C (270 nm), and D (310 nm), can be clearly observed. Band D has a

Table 1. The spectroscopic properties of Ce^{3+} in $Ca_5(PO_4)_3F$.

Property	Value
The position of Ce^{3+} 5d states in excitation curve (nm)	At 20 K: 209 (B), 218 (E), 255 (F), 270 (C), 292 (G), 310 (D) At RT: 212 (B′), 232 (E′), 257 (F′), 271 (C′), 294 (G′), 312 (D′)
The lowest 5d state of Ce^{3+} in Ca(I) site (nm)	310 (20 K)/312 (RT)
The position of emission from Ca(I) site (nm)	408 (two fitted Gaussian sub-bands: 404, and 441 at RT)
The FWHM of emission from Ca(I) site (cm^{-1})	4331 (20 K)
The Stokes shift of Ce^{3+} in Ca(I) site (cm^{-1})	$\sim 7.2 \times 10^3$
The lowest 5d state of Ce^{3+} in Ca(II) site (nm)	292 (20 K)/294 (RT)
The position of emission from Ca(II) site (nm)	353, 330 (RT)
The Stokes shift of Ce^{3+} in Ca(II) site (cm^{-1})	$\sim 3.9 \times 10^3$

maximum at about 310 nm which is assigned to the lowest 4f–5d transition for Ce^{3+} in the host lattice.

As for the assignment of band A, we assume that this band is related to the electronic excitation of PO_4^{3-} anions in the host lattice. The host-related absorption bands of other phosphates and fluorophosphates have been investigated in our previous work [9–11]. Though the compositions and the structure of these phosphates and of the fluorophosphates are different, they all show absorption bands at wavelengths of 150–170 nm. We conclude that the intrinsic absorption of PO_4^{3-} is located around this range. Theoretical calculation [12] has also confirmed that the lowest intramolecular $2t_2 \rightarrow 2a$, $3t_2$ transition energy of the tetrahedral PO_4^{3-} molecule is around 7–10 eV (124–177 nm); the band position that we observed is in this region. Based on above observations, band A is not a 4f–5d transition of Ce^{3+} and therefore band B (209 nm) is attributed to be the highest 4f–5d transition for Ce^{3+} in $Ca_5(PO_4)_3F$.

Ce^{3+} ions have only one outer electron ($4f^1$), and the crystal field may split the excited state ($5d^1$) into at most five components. When more than five 4f–5d absorption bands are observed, this indicates that Ce^{3+} ions occupy more than one lattice site. In curve (a) in addition to the bands B, C and D, shoulder bands E (∼218 nm), F (∼255 nm) and G (∼292 nm) are present. So at least six 4f–5d transition bands are found, which directly suggests that Ce^{3+} ions occupy more than one lattice site in $Ca_5(PO_4)_3F$.

Curve (e) displays the VUV excitation spectrum at RT, and is similar to curve (a). The above-mentioned seven bands are indicated as A′ (∼174 nm), B′ (∼212 nm), C′ (∼271 nm), D′ (∼312 nm), E′ (∼232 nm), F′ (∼257 nm) and G′ (∼294 nm) in figure 2(e). The bands at room temperature have shifted slightly to longer wavelength as compared to the situation at 20 K. Except for the larger difference between band E and E′ the shift is about 2–3 nm. In addition the bands are broader at room temperature, which is the result of the electron–phonon coupling and the temperature dependence of the phonon distribution.

Curves (b), (c), and (d) give the emission spectra under 172 nm VUV and 310 nm UV excitation at 20 K and RT. In each case a broad Ce^{3+} emission band (labelled as I) with a maximum at about 408 nm is observed. This emission has a full-width at half-maximum (FWHM) of ∼4331 cm^{-1} at 20 K. We fitted the emission bands in figures 2(b)–(d) with two Gaussian sub-bands. The reason will be provided later. As an example, the fitted total emission curve (f) and the two fitted Gaussian curves ((g), (h)) peaking at about 404 and 441 nm for curve (d) are displayed in figure 2. All above-mentioned experimental data are summarized in table 1.

The fluoro-apatites $M_5(PO_4)_3F$ (M = Ca, Sr, Ba) belong to the large family of apatite structure compounds with the general formula $M_5(XO_4)_3Y$ ($M^{2+} = Ca^{2+}$, Sr^{2+}, Ba^{2+}, Pb^{2+}, ...; $XO_4^{3-} = PO_4^{3-}$, VO_4^{3-}, ...; $Y^- = F^-$, OH^-, Cl^-, ...) that crystallize in the hexagonal

system with the space group $P6_3/m$. This structure has two cationic M^{2+} sites. 40% of the M^{2+} ions are denoted as M(I) and are at the Wyckoff 4f positions, while the other 60% are denoted as M(II) and are at the Wyckoff 6h positions. M(I) has C_3 point symmetry and is surrounded by nine oxygen anions. M(II) has C_s point symmetry and is surrounded by six oxygen anions plus one F^- anion [13]. A number of rare earth ions were studied in this type of host lattice. Eu^{3+} ions were found to occupy Sr(II) sites of low C_s point symmetry predominantly. A minority of Sr(I) sites with high C_3 symmetry were also occupied by Eu^{3+} [14]. Multi-site occupancy of Nd^{3+} ions was observed in $Ba_5(PO_4)_3F$, and it was estimated that more than 87% of Nd^{3+} ions occupy the Ba(II) site [15]. Spectroscopic studies of $Sr_5(PO_4)_3F$ containing rare earth ions Dy^{3+}, Ho^{3+}, Er^{3+}, Tm^{3+} and Yb^{3+} indicated that the majority of these ions occupy the Sr(II) site [16]. These investigations all suggest that rare earth RE^{3+} (RE = Nd, Eu, Dy, Ho, Er, Tm, and Yb) ions mainly enter the small low-symmetry M(II) sites in $M_5(PO_4)_3F$. However, in the case of the Ca-fluoro-apatite we will show that the emission at 408 nm is mainly related to Ce^{3+} on the Ca(I) sites in $Ca_{5-2x}Ce_xNa_x(PO_4)_3F$ ($x = 0.025$). The reasons are the following.

Although UV excitation and UV-excited emission spectra of Ce^{3+} doped $Ca_5(PO_4)_3F$ were presented before, the VUV excitation and VUV-excited emission spectra were not reported. Gaft [4] found a Ce^{3+} emission band at about 360 nm with short decay time and a band at 430 nm with long decay time. The former was assigned to Ce on a Ca(I) site while the latter was assigned to Ce on a Ca(II) site. Recently, Yang *et al* [5] reported a dominant excitation band at about 296 nm, and the band at 310 nm (D band in figure 2) was not observed. In addition, they observed the main emission band at 334 nm with two shoulder bands at about 354 and 409 nm. The site occupied by Ce was not further discussed in their work.

In order to further investigate the luminescence of Ce^{3+} ions in $Ca_5(PO_4)_3F$ and assign the site occupancy in detail, a series of samples $Ca_{5-2x}Ce_xNa_x(PO_4)_3F$ with different Ce^{3+} concentration was prepared, and the UV excitation and UV-excited emission spectra were studied. Figure 3 shows the UV excitation spectra by monitoring 355 and 406 nm emission, and the emission spectra upon 292 and 313 nm excitation for a series of samples $Ca_{5-2x}Ce_xNa_x(PO_4)_3F$ at RT.

Three excitation bands D (313 nm), G (292 nm) and C (275 nm) are present in curve (a), while two bands G′ (288 nm) and C′ (272 nm) are present in curve (c) of figure 3. The positions of all these bands are in line with those in figures 2(a) and (e) that were assigned to Ce^{3+} 4f–5d transitions. The emission under 313 nm excitation is the same as when excited in the phosphate band at 172 nm. Different characteristics are observed in figure 3(d) upon 292 nm excitation. At low Ce^{3+} concentration, for example when $x = 0.005$, the emission at 355 nm is dominant. The band (curve 1) has a shoulder on its short-wavelength side and a tail on its long-wavelength side. With increasing x value, the long-wavelength emission at 408 nm increases progressively. And then, at $x = 0.05$, concentration quenching leads to a decrease of the emission at both 355 and 408 nm. The concentration quenching is also observed under 313 nm excitation in figure 3(b).

As mentioned above, there are two types of Ca^{2+} site in $Ca_5(PO_4)_3F$. Because of the large energy difference, the emission bands at 355 nm (marked as II) and 408 nm (marked as I) are surely from Ce^{3+} on the two different Ca^{2+} sites. Upon 313 nm (band D in figure 3(a)) excitation, only emission at 408 nm (band I) is seen in figure 3(b), which suggests that the excitation band D and the emission band I belong to the same Ce site. Similarly, excitation band G′ and emission band II are from the same but another Ce^{3+} site, as shown in figures 3(c) and (d).

Next we will assign the Ce^{3+} on Ca^{2+} sites responsible for bands D/I and G′/II in figure 3. The large nine-fold coordinated Ca(I) sites are in the form of a tricapped trigonal prism. It is usually observed that Ce^{3+} with this form of coordination shows an emission with an

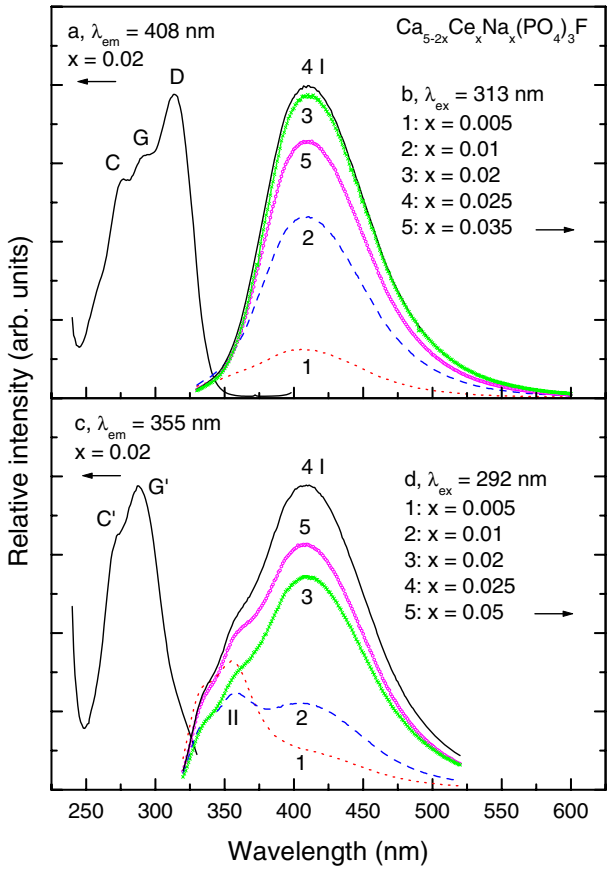

Figure 3. The UV excitation spectra and the emission spectra under UV excitation for the series of samples $Ca_{5-2x}Ce_xNa_x(PO_4)_3F$ with different x values at RT.

exceptionally large Stokes shift [17]. The two Gaussian sub-bands of band I are at 404 and 441 nm, so the Stokes shift with the lowest excitation band at 313 nm is 7.2×10^3 cm^{-1}. The emission band II in figure 3(d) can be described by two Gaussian curves at 330 and 353 nm. With the first excitation band at about 292 nm a Stokes shift of 3.9×10^3 cm^{-1} is found. We attribute band D (313 nm) to the lowest 5d state of Ce^{3+} in Ca(I) sites, and the emission from Ca(I) sites is with a maximum at 408 nm. We attribute band G (292 nm) to the lowest 5d state of Ce^{3+} in Ca(II) sites, and the emission from Ca(II) sites is with a maximum at 330 and 353 nm. These attributions are further motivated by the lower degree of covalency around the Ca(II) site due to the presence of an F^- anion in the coordination sphere leading to higher average energy of the 5d configuration.

Upon 292 nm excitation of the Ce^{3+} at Ca(II) sites, emission at 330 and 353 nm from Ce^{3+} at Ca(II) sites as well as 408 nm from Ce^{3+} at Ca(I) sites is observed, which indicates efficient energy transfer from Ce(II) to Ce(I). In contrast, upon 313 nm excitation of the Ce^{3+} at Ca(I) sites, only the emission at 408 nm from Ce^{3+} at Ca(I) sites is observed, suggesting that energy transfer from Ce(I) to Ce(II) is inefficient. From figures 3(b) and (d), it is observed that the emission bands of Ce(II) are better resolved than that of Ce(I), which is directly related with the large Stokes shift of Ce(I) emission.

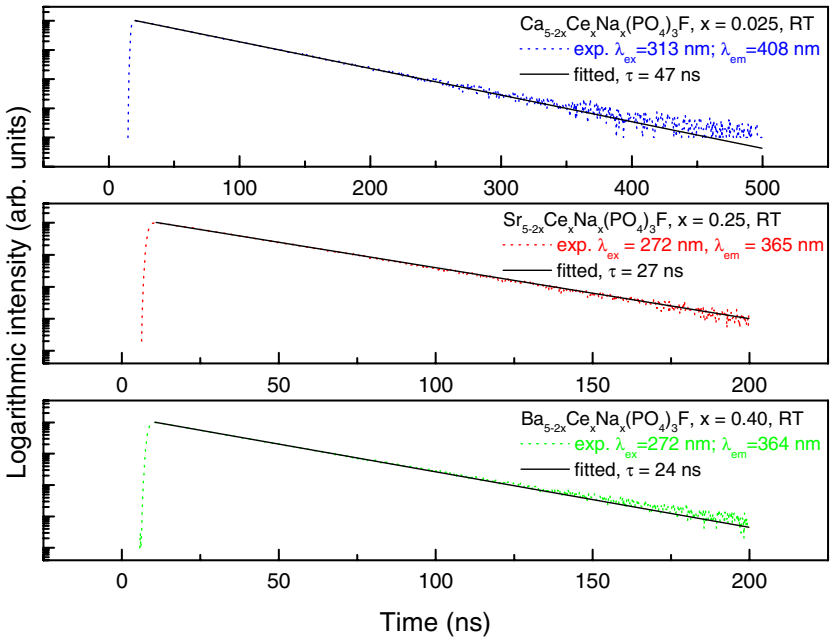

Figure 4. The decay curve of samples $Ca_{5-2x}Ce_xNa_x(PO_4)_3F$ ($x = 0.025$, curve (a)), $Sr_{5-2x}Ce_xNa_x(PO_4)_3F$ ($x = 0.25$, curve (b)) and $Ba_{5-2x}Ce_xNa_x(PO_4)_3F$ ($x = 0.40$, curve (c)) displayed on a logarithmic intensity scale at RT.

The ionic radii of seven-fold coordinated Ca^{2+} and Ce^{3+} ions are 106 and 107 pm, and of nine-fold coordinated Ca^{2+} and Ce^{3+} ions are 118 and 119 pm, respectively [18]. Clearly the radii of Ce^{3+} and Ca^{2+} are similar to each other in either seven-fold or nine-fold coordination. Because of this, Ce^{3+} ions can enter both Ca(I) and Ca(II) sites. From our experiments, we conclude that Ce^{3+} ions enter Ca(II) sites preferentially at low concentration, and the occupation of Ca(I) sites becomes more important with increase of Ce^{3+} concentration.

The decay curve of Ce^{3+} emission for sample $Ca_{5-2x}Ce_xNa_x(PO_4)_3F$ ($x = 0.025$) at RT is shown in figure 4(a); the curve can be well fitted by a single exponential equation, $I_t = I_0 \exp(-t/\tau)$, where I_t and I_0 are the luminescence intensity at time t and time 0, and τ is the decay time. The value of τ is found to be 47 ns from the fitted curve. In the curve, no energy transfer process between luminescent centres from different lattice sites Ca(I) and Ca(II) was observed. This agrees with our standpoint that the excitation bands D (310 nm in curve (a)) and D′ (313 nm in curve (e)) as well as the emission band at 408 nm (in curves (b)–(d)) in figures 2 and 3 are from Ce^{3+} ions at the same Ca(I) lattice site.

3.3. VUV–vis luminescence of $Sr_5(PO_4)_3F$:Ce

The spectroscopic curves in the 130–450 nm range for sample $Sr_{5-2x}Ce_xNa_x(PO_4)_3F$ ($x = 0.25$) were measured at RT and are displayed in figure 5. Curve (a) is the emission spectrum under 212 nm excitation. A broad band with a maximum at about 343 nm and a shoulder band on the long-wavelength side can be observed. This emission band can be fitted with two Gaussian sub-bands peaking at 336 and 360 nm. The energy difference of the sub-bands is about 1984 cm^{-1}, which is close to the ^2F_J ($J = 7/2, 5/2$) energy gap of Ce^{3+} ($\sim$2000 cm^{-1}) in most Ce^{3+} activated phosphors, indicating that the emission of Ce^{3+} ions in $Sr_5(PO_4)_3F$ is from a single lattice site.

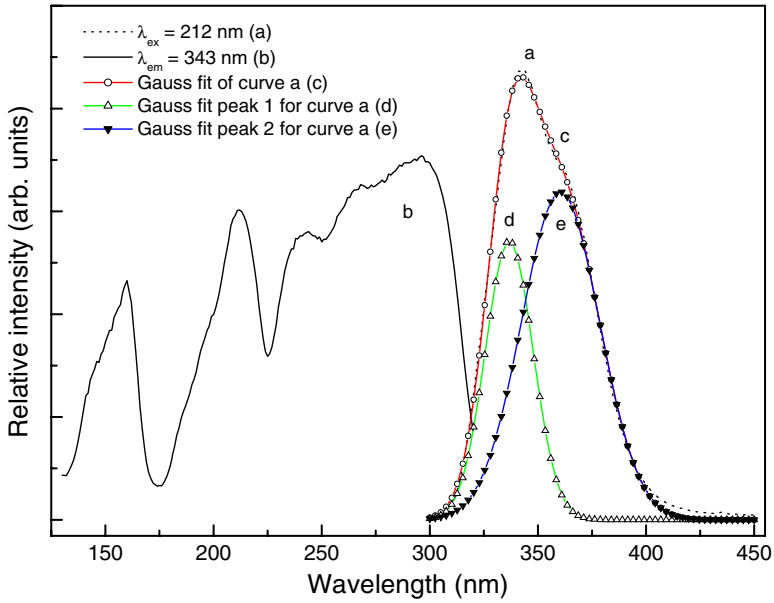

Figure 5. The excitation spectrum and the emission spectrum for samples $Sr_{5-2x}Ce_xNa_x(PO_4)_3F$ ($x = 0.25$) at RT.

The excitation curve (b) can be divided into two parts. The band below 175 nm is the host-related absorption as discussed in section 3.2, whereas the bands above 175 nm are f–d transitions of Ce^{3+} in the host lattice. The f–d transitions in figure 5(b) are less resolved as those in figures 2(a) and (e). However, on comparing figures 5(b) and 2(a), (e) in more detail, it can be observed that the lowest 5d state for Ce^{3+} in $Sr_5(PO_4)_3F$ is at about 296 nm, which is near the band G/G′ in $Ca_5(PO_4)_3F$:Ce^{3+}; see figures 2 and 3. The doublet emission bands at 336 and 360 nm for Ce^{3+} in $Sr_5(PO_4)_3F$ are close to the emission of Ce^{3+} in Ca(II) sites (330 and 353 nm) of $Ca_5(PO_4)_3F$. The Stokes shift of Ce^{3+} in $Sr_5(PO_4)_3F$ is about 4.0×10^3 cm^{-1}, which is also close to the value of 3.9×10^3 cm^{-1} for Ce^{3+} on Ca(II) sites of $Ca_5(PO_4)_3F$. If we take into account the uncertainties, both are nearly the same value. These observations suggest that the luminescence of Ce^{3+} in $Sr_5(PO_4)_3F$ is mainly from Sr(II) sites even at high concentration. As the size of Sr^{2+} is larger than that of Ce^{3+}, it is likely that Ce^{3+} prefers to occupy the smaller Sr(II) sites in $Sr_5(PO_4)_3F$.

Figure 4(b) shows the decay curve of Ce^{3+} emission in $Sr_{5-2x}Ce_xNa_x(PO_4)_3F$ ($x = 0.25$) at RT. The curve was fitted by a single exponential decay with $\tau \approx 27$ ns. The smaller value as compared to 47 ns for Ce^{3+} in $Ca_5(PO_4)_3F$ in figure 4(a) is in line with the shorter wavelength of emission as predicted by the theoretical decay rate formula [19]. The influence of the concentration of dopant Ce^{3+} ions on the decay time is known, but the decay time is coincident with the theoretical decay rate formula in the present case, though the two samples have different doping concentration.

3.4. VUV–vis luminescence of $Ba_5(PO_4)_3F$:Ce

Figure 6 presents the spectroscopic curves in the 130–600 nm range for samples $Ba_{5-2x}Ce_xNa_x(PO_4)_3F$ ($x = 0.40$) at RT. Curves (a) and (b) are the emission spectra upon 272 and 172 nm excitation, respectively. The curves consist of a doublet band peaking at about

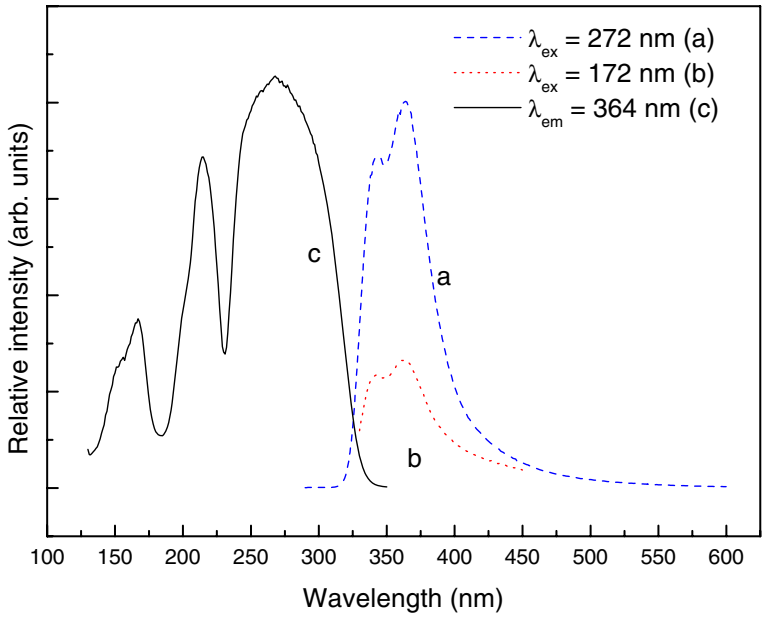

Figure 6. The excitation spectrum and the emission spectra for samples $Ba_{5-2x}Ce_xNa_x(PO_4)_3F$ ($x = 0.40$) at RT.

342 and 364 nm. The two bands correspond to the 5d–^2F_J ($J = 5/2, 7/2$) transitions of Ce^{3+} ions. As for $Sr_5(PO_4)_3F$, we attribute the emission to Ce^{3+} on the smaller Ba(II) sites of $Ba_5(PO_4)_3F$. The doublet band from Ca(II) sites was found at about 330 and 353 nm, and that of Sr(II) sites at 336 and 360 nm. Therefore a slight red shift of Ce(II) emission occurs with smaller cation size from Ca to Sr to Ba.

The decay curve of Ce^{3+} emission for sample $Ba_{5-2x}Ce_xNa_x(PO_4)_3F$ ($x = 0.40$) at RT is shown in figure 4(c). The decay time τ is about 24 ns, the smallest value among the phosphors $M_{5-2x}Ce_xNa_x(PO_4)_3F$ (M = Ca, Sr, Ba). The doping concentration of Ce^{3+} in samples $M_{5-2x}Ce_xNa_x(PO_4)_3F$ (M = Ca, Sr, Ba) will have an influence on the decay time. It is necessary to study the relationship between doping concentration and the decay time systematically. Further investigation on this issue is in progress.

3.5. X-ray excited luminescence of $Ca_5(PO_4)_3F$:Ce, $Sr_5(PO_4)_3F$:Ce and $Ba_5(PO_4)_3F$:Ce

X-ray excited emission spectra of $M_5(PO_4)_3F$:Ce^{3+} (M = Ca, Sr, Ba) recorded at room temperature (RT) are shown in figure 7. The spectra together with that of a BaF_2 reference sample were measured under the same experimental conditions. The bands above 470 nm in figures 7(c) and (d) are from Eu^{3+} or other unknown impurities. The $Ca_{5-2x}Ce_xNa_x(PO_4)_3F$ ($x = 0.025$) sample exhibits a broad band at 412 nm with a shoulder band at 354 nm, the $Sr_{5-2x}Ce_xNa_x(PO_4)_3F$ ($x = 0.25$) sample shows a broad emission band around 342 nm and $Ba_{5-2x}Ce_xNa_x(PO_4)_3F$ ($x = 0.40$) shows a broad band at about 358 nm, which are in line with the positions observed in figures 3, 5 and 6. The bands are assigned to the f–d transitions of Ce^{3+} in the host lattices.

An estimate for the x-ray excited absolute light yield output of the samples of figure 7 was made from the ratio of the integrated intensity from those samples with that of the BaF_2 reference sample. With the methods outlined in [20] we found for our reference BaF_2 crystal a light output of about 9300 photons per 1 MeV absorbed gamma-ray energy. From

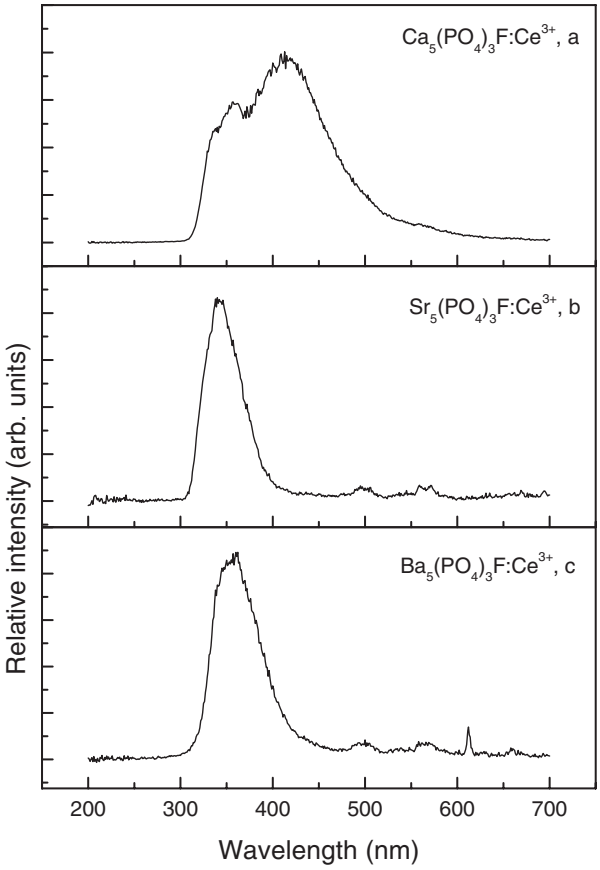

Figure 7. The x-ray excited emission spectra of samples $Ca_{5-2x}Ce_xNa_x(PO_4)_3F$ ($x = 0.025$), $Sr_{5-2x}Ce_xNa_x(PO_4)_3F$ ($x = 0.25$), and $Ba_{5-2x}Ce_xNa_x(PO_4)_3F$ ($x = 0.40$) at RT.

that we estimate rather low x-ray photon yields for $Sr_{5-2x}Ce_xNa_x(PO_4)_3F$ ($x = 0.20$) and $Ba_{5-2x}Ce_xNa_x(PO_4)_3F$ ($x = 0.40$) of about 340 and 400 photons/MeV, respectively. A relatively high value of 3200 photons/MeV was found for sample $Ca_{5-2x}Ce_xNa_x(PO_4)_3F$ ($x = 0.025$). We suppose that the doping concentration of Ce^{3+} in samples $M_{5-2x}Ce_xNa_x(PO_4)_3F$ (M = Ca, Sr, Ba) will have an influence on the light yield of Ca-/Sr-/Ba-containing phosphor. Further investigation on this issue is probably beneficial to make some physical conclusions, but from the above light output values, we estimate that these types of phosphors are not well suited for x-ray or gamma-ray phosphors.

4. Conclusions

A series of phosphors with molecular formulae $M_{5-2x}Ce_xNa_x(PO_4)_3F$ (M = Ca, Sr, Ba) was prepared by a high-temperature solid-state reaction technique. The spectroscopic properties in the VUV–vis range were investigated and discussed. It is found that Ce^{3+} ion predominantly enters Ca(II) sites when the dopant concentration is low. The occupancy of Ca(I) sites increases with increasing Ce concentration in samples $Ca_{5-2x}Ce_xNa_x(PO_4)_3F$. The Sr(II)/Ba(II) sites are mainly occupied in $Sr_{5-2x}Ce_xNa_x(PO_4)_3F$ and $Ba_{5-2x}Ce_xNa_x(PO_4)_3F$ even at higher dopant concentration. The x-ray excited luminescence of $M_5(PO_4)_3F:Ce^{3+}$ for M = Sr and Ba were measured, and the highest light output was found in $Ca_5(PO_4)_3F:Ce^{3+}$, which is related to both the Ca(I) and Ca(II) site occupancy of Ce^{3+} in the host.

Acknowledgments

The work is financially supported by the National Natural Science Foundation of China (Grant No 20571088), by the Science and Technology Project of Guangdong province (Grant Nos 2005A10609001, 2005B10301016) and by the NSRL innovation foundation from the Ministry of Education of China (Grant No 20051251S).

References

[1] Blasse G 1975 Influence of local charge compensation on site occupation and luminescence of apatites *J. Solid State Chem.* **14** 181–4

[2] Pappalardo R G, Walsh J and Hunt R B Jr 1983 Cerium-activated halophosphate phosphors *J. Electrochem. Soc.* **130** 2087–96

[3] Kottaisamy M, Jagannathan R, Jeyagopal P, Rao R P and Narayanan R L 1994 Eu^{2+} luminescence in $M_5(PO_4)_3X$ apatites, where M is Ca^{2+}, Sr^{2+} and Ba^{2+}, and X is F^-, CI^-, Br^- and OH^- *J. Phys. D: Appl. Phys.* **27** 2210–5

[4] Gaft M, Panczer G, Reisfeld R and Uspensky E 2001 Laser-induces time-resolved luminescence as a tool for rare-earth element identification in minerals *Phys. Chem. Minerals* **28** 347–63

[5] Yang P, Yao G Q and Lin J H 2004 Photoluminescence of Ce^{3+} in haloapatites $Ca_5(PO_4)_3X$ *Inorg. Chem. Commun.* **7** 302–4

[6] Duan C J, Wu X Y, Liu W, Chen H H, Yang X X and Zhao J T 2005 X-ray excited luminescent properties of apatitic compounds $Ba_5(PO_4)_3X$ (X: OH^-, Cl^-, Br^-); structure and hydroxyl ion conductivity of barium hydroxylapatite *J. Alloys Compounds* **396** 86–91

[7] Dominiak-Dzik G, Ryba-Romanowski W, Koács L and Beregi E 2004 Effect of temperature on luminescence and VUV to visible conversion in the $YAl_3(BO_3)_4$:Dy^{3+} (YAB:Dy) crystal *Radiat. Meas.* **38** 557–61

[8] Lin H H, Liang H B, Tian Z F, Su Q, Xie H Y, Ding J F, Zhang G B and Fu Y B 2006 Vacuum-ultraviolet–vis luminescence of dibarium magnesium orthoborate $Ba_2Mg(BO_3)_2$ doped with Ce^{3+} and Eu^{2+} ions *J. Mater. Res.* **21** 864–9

[9] Tian Z F, Liang H B, Lin H H, Su Q, Guo B, Zhang G B and Fu Y B 2006 Luminescence of $NaGdFPO_4$:Ln^{3+} after VUV excitation: a comparison with $GdPO_4$:Ln^{3+} (Ln = Ce, Tb) *J. Solid State Chem.* **179** 1356–62

[10] Liang H B, Tao Y, Su Q and Wang S B 2002 VUV–UV photoluminescence spectra of strontium orthophosphate doped with rare earth ions *J. Solid State Chem.* **167** 435–40

[11] Liang H B, Tao Y, Xu J H, He H, Wu H, Chen W X, Wang S B and Su Q 2004 Photoluminescence of Ce^{3+}, Pr^{3+} and Tb^{3+} activated $Sr_3Ln(PO_4)_3$ under VUV–UV excitation *J. Solid State Chem.* **177** 901–8

[12] Saito S, Wada K and Onaka R 1974 Vacuum ultraviolet reflection spectra of KDP and ADP *J. Phys. Soc. Japan* **37** 711–5

[13] Gaft M, Reisfeld R, Panczer G, Boulon G, Shoval S and Champagnon B 1997 Accommodation of rare-earths and manganese by apatite *Opt. Mater.* **8** 149–56

[14] Wright A O, Seltzer M D, Gruber J B and Chai B H T 1995 Site-selective spectroscopy and determination of energy levels in Eu^{3+}-doped strontium fluorophosphate *J. Appl. Phys.* **78** 2456–67

[15] Loutts G B, Bonner C, Meegoda C, Ries H, Noginov M A, Noginova N, Curley M, Venkateswarlu P, Rapaport A and Bass M 1997 Crystal growth, spectroscopic characterization, and laser performance of a new efficient laser material Nd:$Ba_5(PO_4)_3F$ *Appl. Phys. Lett.* **71** 303–5

[16] Gruber J B, Zandi B and Merkle L 1998 Crystal-field splitting of energy levels of rare-earth ions Dy^{3+} ($4f^9$) and Yb^{3+} ($4f^{13}$) in M(II) sites in the fluorapatite crystal $Sr_5(PO_4)_3F$ *J. Appl. Phys.* **83** 1009–17

[17] Dorenbos P 2000 5d-level energies of Ce^{3+} and the crystalline environment. I. Fluoride compounds *Phys. Rev.* B **62** 15640–9

[18] Shannon R D 1976 Revised effective ionic radii and systematic studies of interatomic distances in halides and chalcogenides *Acta Crystallogr.* A **32** 751–67

[19] Dorenbos P 2002 Light output and energy resolution of Ce^{3+}-doped scintillators *Nucl. Instrum. Methods* A **486** 208–13

[20] de Haas J T M, Dorenbos P and van Eijk C W E 2005 Measuring the absolute light yield of scintillators *Nucl. Instrum. Methods Phys. Res.* A **537** 97–100